Giant excitonic effects in vacancy-ordered double perovskites

Fan Zhang,[1] Weiwei Gao,[1,*] Greis J. Cruz,[2] Yi-yang Sun,[3] Peihong Zhang,[2,†] and Jijun Zhao[1]

[1]*Key Laboratory of Material Modification by Laser, Ion, and Electron Beams, Dalian University of Technology, Ministry of Education, Dalian 116024, China*

[2]*Department of Physics, State University of New York at Buffalo, Buffalo, New York 14260, USA*

[3]*State Key Laboratory of High Performance Ceramics and Superfine Microstructure, Shanghai Institute of Ceramics, Chinese Academy of Sciences, Shanghai 201899, China*

(Received 9 October 2022; accepted 23 May 2023; published 9 June 2023)

Using first-principles *GW* plus Bethe-Salpeter equation calculations, we identify exceptionally strong excitonic effects in several vacancy-ordered double perovskites Cs_2MX_6 (M = Ti, Zr; X = I, Br). Giant exciton binding energies of about 1 eV are found in these moderate-gap, inorganic bulk semiconductors, pushing the limit of our understanding of the electron-hole interaction and exciton formation in solids. Not only are the exciton binding energies extremely large compared with any other moderate-gap bulk semiconductors, but they are also larger than typical two-dimensional semiconductors with comparable quasiparticle gaps. Our calculated lowest bright exciton energies agree well with the measured optical band gaps. The low-energy excitons closely resemble the Frenkel excitons in molecular crystals, as they are highly localized in a single $[MX_6]^{2-}$ octahedron and extended in the reciprocal space. The weak dielectric screening effects and the nearly flat frontier electronic bands, which are derived from the weakly coupled $[MX_6]^{2-}$ units, together explain the significant excitonic effects. Spin-orbit coupling effects play a crucial role in redshifting the lowest bright exciton by mixing up spin-singlet and spin-triplet excitons, while exciton-phonon coupling effects have minor impacts on the calculated exciton binding energies.

DOI: 10.1103/PhysRevB.107.235119

I. INTRODUCTION

An exciton is a composite boson consisting of a correlated electron-hole (*e-h*) pair bound by screened Coulomb interaction. The attractive Coulomb interaction between electrons and holes creates low-lying excitons with energy E_{ex} below the quasiparticle (QP) band gap E_g^{QP}. Systems with large exciton binding energies are important for exploring light-matter interactions as well as for developing exciton-based optoelectronic devices operating at room temperature [1–8]. They are also potential hosts for composite quasiparticles such as biexcitons [9,10], trions [11,12], and exciton polaritons [13,14], which have been extensively studied during the last decade. Excitonic effects also profoundly impact the performance of optoelectronic materials such as quasi-two-dimensional (2D) hybrid perovskites [15–17].

Well-known examples of materials with strong excitonic effects include low-dimensional materials [18–21], molecular crystals [22,23], and alkaline halides [24,25]. The latter two are bulk materials that can host strongly bound Frenkel or charge-transfer excitons. On the other hand, Wannier-Mott excitons in most inorganic bulk semiconductors with moderate band gaps ($E_g < 4$ eV) have small exciton binding energies ranging from a few meV to 100 meV [26–28]. Notably, cuprous chloride and cuprous oxide, which have been extensively studied for realizing Bose-Einstein condensation of excitons, possess large exciton binding energy of nearly 200 meV [29–31]. Other inorganic semiconductors with large exciton binding energies include delafossites (E_b^{ex} = 0.3–0.5 eV) [32,33] and quasi-2D perovskites [34–36]; all of them have quasilayered structures.

Owing to the rich choices of chemical composition, tunable optical band gap, nontoxicity, and earth abundance, the vacancy-ordered double perovskites (VODPs) have been proposed as promising materials for photovoltaic applications [37–39]. In this paper, using density functional theory (DFT) [40] and many-body perturbation theory [41,42], we investigate the quasiparticle and excitonic properties of a group of VODPs, including Cs_2TiX_6 and Cs_2ZrX_6 (X = I, Br). Our combined *GW* and Bethe-Salpeter equation (BSE) [43–48] calculations reveal an extremely strong excitonic effect with exciton binding energies (≈1 eV) far exceeding those in any other known moderate-gap bulk semiconductors. The discovery of three-dimensional (3D) all-inorganic semiconductors with moderate gaps and strong excitonic effects not only broadens our understanding of the *e-h* interaction in solids but may also guide the future search for bulk systems with large exciton binding energies. It should be mentioned that recent studies showed a surprisingly large discrepancy (over 1 eV) between the calculated fundamental band gaps of Cs_2TiI_6 and Cs_2ZrI_6 and the measured values [37,49]. The overestimation of fundamental band gaps was ascribed to improper treatment of localized Ti 3*d* orbitals within the *GW* approximation [37]. Our results clearly show that it is the surprisingly

*weiweigao@dlut.edu.cn
†pzhang3@buffalo.edu

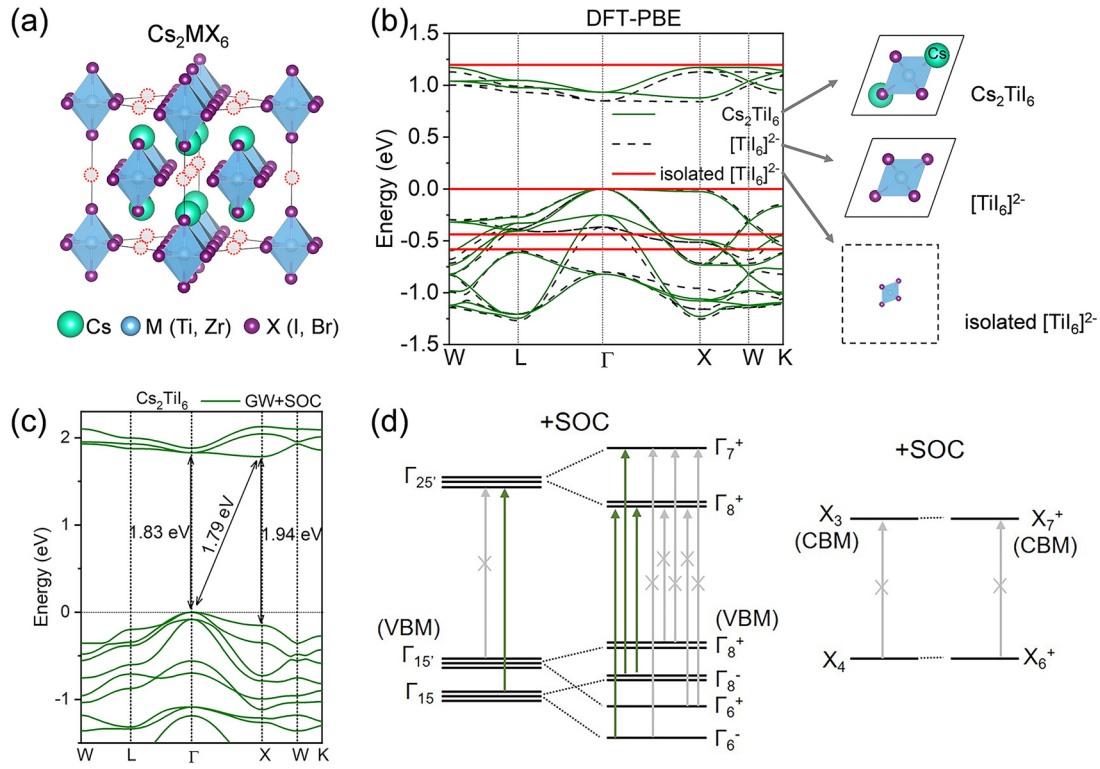

FIG. 1. (a) Crystal structures of Cs_2MX_6 showing the weakly coupled $[TiI_6]^{2-}$ octahedral units. The red dotted circles show M vacancies. (b) DFT-PBE band structures of Cs_2TiI_6 crystal (green solid curves), $[TiI_6]^{2-}$ crystal (dashed black curve), and isolated $[TiI_6]^{2-}$ molecule (red lines). The highest occupied states are shifted to zero. (c) Quasiparticle band structure of Cs_2TiI_6 including the SOC effects. (d) A schematic diagram showing the spin-orbit splitting and allowed optical transitions at the Γ and X points of Cs_2TiI_6.

strong excitonic effects in these materials that are responsible for the large difference between quasiparticle and optical gaps.

II. RESULTS AND DISCUSSION

A. Crystal structure and frontier electronic structure

The crystal structure of Cs_2MX_6 (M = Ti, Zr; X = I, Br) VODP can be visualized by removing every other M-site cation from the $CsMX_3$ perovskite structure, thus the name of vacancy-ordered double perovskite [38,49], as shown in Fig. 1(a) in which the dotted red circles indicate the ordered vacancies. We mentioned that VODPs are a class of well-characterized, stable complex halides with the general composition A_2MX_6 (A = Cs) [37–39]. The $[MX_6]^{2-}$ octahedral clusters in VODP Cs_2MX_6 do not form covalent bonds with one another because they are separated by the evenly distributed M-site vacancies. The band structures of these four VODPs are quite similar (Fig. S1 in Supplemental Material [50]), and replacing Ti (I) with Zr (Br) in Cs_2MX_6 increases the fundamental band gap [37]. Both Cs_2TiX_6 and Cs_2ZrX_6 have an indirect band gap between the valence band maximum at Γ and the conduction band minimum at X. The low-energy conduction bands are mainly derived from the M-site d states, whereas the highest valence bands are mostly contributed by the halogen element X. Under the influence of the octahedral crystal field, the d-derived conduction bands split into a doublet and a triplet group; the low-energy triplet bands are fairly flat with an extremely narrow band width (0.29, 0.25, 0.44, and 0.37 eV for Cs_2TiI_6, Cs_2TiBr_6, Cs_2ZrI_6, and Cs_2ZrBr_6, respectively). The top valence band is virtually dispersionless from Γ to X, and the direct gap of Cs_2TiI_6 at Γ is only 40 meV larger than the indirect gap between Γ and X.

In order to facilitate later discussion and to better illustrate the roles of Cs^+ and $[MX_6]^{2-}$ in defining the frontier states, we compare the DFT band structure of Cs_2TiI_6 with those of two fictitious systems, namely, a periodic system of $[TiI_6]^{2-}$ without the Cs^+ ions (with the same lattice constant as Cs_2TiI_6) and an isolated $[TiI_6]^{2-}$ octahedron, as shown in Fig. 1(b). The DFT band structures are calculated using the Perdew-Burke-Ernzerhof (PBE) functional within the QUANTUM ESPRESSO package (after Refs. [51–54]; for details of the calculations, see the Supplemental Material [50]). The nearly identical frontier band structures of Cs_2TiI_6 and $[TiI_6]^{2-}$ suggest that Cs^+ ions merely function as electron donors and spacers without significantly affecting the band dispersion of the system. The role of Cs^+ here is similar to that of $CH_3NH_3^+$ in $CH_3NH_3PbI_3$ [55]. The highest-occupied molecular orbital (HOMO) of $[TiI_6]^{2-}$ is mostly composed of the iodine 5p orbitals, while the titanium 3d orbitals dominate the lowest-unoccupied molecular orbital (LUMO). These $[TiI_6]^{2-}$ derived LUMO and HOMO states interact to form the lowest conduction bands and highest valence bands of Cs_2TiI_6, respectively. The narrow widths of the frontier energy bands in Cs_2TiI_6 further suggest that $[TiI_6]^{2-}$ behaves like a polyatomic superanion [56], which interacts weakly with itself. In this manner, Cs_2TiI_6 crystal can be understood as an assembly of $[TiI_6]^{2-}$ units and Cs^+ spacers. As we will discuss below,

TABLE I. Quasiparticle, excitonic, and dielectric properties of four VODPs. Energy gaps are in eV.

		Cs_2TiI_6	Cs_2TiBr_6	Cs_2ZrI_6	Cs_2ZrBr_6
QP gap (*GW*)	Γ-Γ	1.83	3.35	3.22	4.97
	X-*X*	1.94	3.40	3.36	5.03
	X-Γ	1.79	3.31	3.20	4.95
Opt. gap (exp)		1.02	2.00		3.76
E_{ex}^{Bright}		1.04	2.03	2.33	3.59
E_{ex}^{Dark}		0.85	1.66	2.18	3.28
E_b^{Bright}		0.79	1.32	0.89	1.38
E_b^{Dark}		0.98	1.69	1.04	1.69
ε_∞		4.46	3.26	3.68	2.97
ε_0		11.27	8.59	11.89	8.90
ω_{LO} (meV)		27.91	34.50	24.40	30.14
ΔE_b (meV)		–32.8	–42.0	–32.9	–39.5

such a unique structure is responsible for extremely strong excitonic effects in VODPs.

B. Quasiparticle and SOC effects

The QP band structure of Cs_2TiI_6 is calculated using the BERKELEYGW package [43–48] as shown in Fig. 1(c). The indirect QP band gap of Cs_2TiI_6 is 1.79 eV, which is slightly smaller than the direct band gap at Γ (1.83 eV). The calculated QP band gap within the G_0W_0 approximation is significantly larger than the measured optical gap of 1.02 eV [49]. It is noteworthy that our calculated QP gap is smaller than that reported in a previous work [37] by 0.54 eV. This discrepancy mainly stems from the use of different cutoff parameters and treatment of the frequency-dependent dielectric function [57–60]. Indeed, a small cutoff of dielectric matrices used in *GW* calculations can lead to an overestimation of the quasiparticle band gap by as much as 0.5 eV (Fig. S2 in Supplemental Material [50]). We also compare the QP band gaps of all four VODPs in Table I and the DFT-PBE band structures in Fig. S1 of Supplemental Material [50].

A comparison of the band structures calculated with and without spin-orbit coupling (SOC) (Fig. S1 of Supplemental Material [50]) reveals strong relativistic effects on the top valence bands, and the gap at the Γ point of Cs_2TiI_6 is reduced by about 130 meV due to the SOC effects. Figure 1(d) highlights the impacts of the SOC effects on the frontier electronic states at the Γ and *X* points of Cs_2TiI_6. If the SOC effects are neglected, the lowest-energy direct transitions at the Γ and *X* points ($\Gamma_{15'} \rightarrow \Gamma_{25'}$ and $X_4 \rightarrow X_3$) are dipole forbidden, while the second lowest-energy direct transition at the Γ point ($\Gamma_{15} \rightarrow \Gamma_{25'}$) is dipole allowed [61]. After the SOC effects are considered, the triply degenerate states split into a quadruplet and a doublet (including Kramer's degeneracy). The dipole-allowed optical transitions are indicated by green arrows in Fig. 1(d). Due to the SOC splitting, the energy of the dipole-allowed transition $\Gamma_8^- \rightarrow \Gamma_8^+$ is smaller than that of $\Gamma_{15} \rightarrow \Gamma_{25'}$ by about 0.31 eV. In the following, we show that this trend also holds when the excitonic effects are considered.

C. Optical absorption spectra

Figure 2(a) shows the imaginary part of the frequency-dependent dielectric constant of Cs_2TiI_6, calculated with and without including the *e*-*h* interaction. Our *GW* + BSE calculations reveal several prominent excitonic absorption peaks far below the quasiparticle band gap. In fact, the lowest-energy exciton locates at 0.85 eV, indicating a giant binding energy of nearly 1 eV and the formation of Frenkel excitons. The lowest-energy exciton is a dark exciton with a negligible optical dipole moment, while the lowest-energy bright exciton locates at 1.04 eV, agreeing well with the measured optical gap of 1.02 eV [49]. We have carefully checked the convergence of the calculated exciton binding energies and absorption spectra and found that the results converge quickly with respect to the density of the *k*-point sampling (as shown in Table S1 and Fig. S3 of Supplementary Material [50]). In contrast, binding energies of Wannier excitons in bulk and 2D systems often require extremely dense *k* grids to achieve proper convergence [62,63]. As we will show later, the *e*-*h* amplitudes of the low-energy excitons spread across a large part of the Brillouin zone (BZ), which explains the rapid convergence behavior of the calculated exciton binding energy.

The strong SOC effects on the calculated band structure, especially on the top valence states as shown in Fig. 1(c), result in significant changes in the calculated excitonic structure and optical absorption. To uncover the effects of SOC on the low-energy excitons, we compare the excitonic structures calculated with and without the SOC effects. When the SOC effects are neglected, an excitonic state can be either spin-0 (singlet) or spin-1 (triplet). The triplet excitons are always dark since spin is conserved in optical dipole transitions if the SOC effects are neglected. The excitation energies of the singlet and triplet excitons for Cs_2TiI_6 are shown in Fig. 2(b), in which each vertical line corresponds to an excitonic state; these lines are color coded according to their brightness, i.e., the square of the dipole matrix elements. The lowest-energy triplet exciton is about 0.1 eV lower than the lowest-energy singlet one, which is also a dark exciton due to the orbital symmetry as discussed earlier. The lowest-energy bright exciton is located at around 1.34 eV and can be attributed to the $\Gamma_{15} \rightarrow \Gamma_{25'}$ transitions shown in Fig. 1(d).

When the SOC effects are considered, the excitonic states are a mixture of spin singlets and spin triplets [45]. The lowest-energy exciton, which is mainly derived from the low-energy spin-triplet states, is dark, as shown in Fig. 2(c). Moreover, the SOC effects cause a significant redshift (from 1.34 to 1.04 eV) of the absorption edge, bringing theory in better agreement with experiment [49]. The exciton binding energy of Cs_2TiI_6 ($E_b^{ex} = 0.98$ eV) is nearly twice that of monolayer 2H-$MoSe_2$ ($E_b^{ex} = 0.55$ eV) [5], which has a comparable quasiparticle gap ($E_g = 2.1$ eV). This finding is rather surprising, as it is well known that the excitonic effects in bulk semiconductors are often much weaker than those in 2D semiconductors [64–66] owing to the stronger screening effect in 3D solids.

The calculated energies of the lowest-energy bright excitons for the other three VODPs (Cs_2TiBr_6, Cs_2ZrI_6, and Cs_2ZrBr_6) also agree well with the experimental optical gaps, as summarized in Table I. The imaginary parts of the dielectric

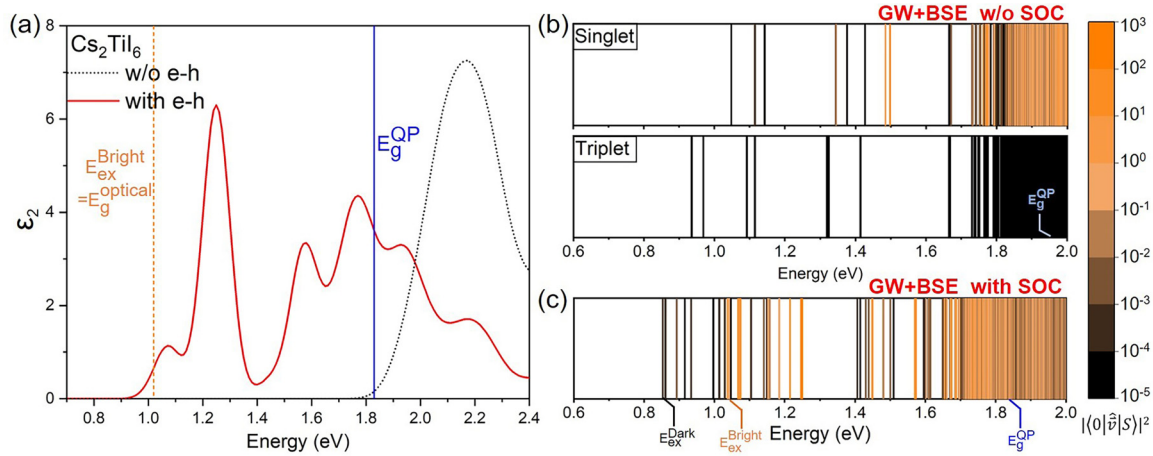

FIG. 2. (a) The imaginary part of the dielectric function of Cs_2TiI_6, calculated without (black dashed line) and with (red solid line) *e-h* interactions. A Gaussian broaden of 0.05 eV is used in the calculations. The lowest-energy bright exciton and fundamental band gap are marked in orange and blue lines, respectively. (b) Energies of singlet and triplet excitons. (c) Energies of excitons calculated with the SOC effects.

functions of these three VODPs are compared in Figs. S4–S6 of Supplemental Material [50]. In addition, we compared the calculated absorption spectra of Cs_2TiI_6 with the experimental results [67], which achieved best match, as shown in Fig. S9 of Supplemental Material [50]. Similar to the case of Cs_2TiI_6, the lowest-energy excitons of these three VODPs are also dark, and the corresponding exciton binding energies are extremely large. Perhaps the most striking finding is the binding energy of the lowest dark exciton in Cs_2ZrBr_6, which reaches 1.69 eV.

D. Characters of low-energy excitons

The abnormally large exciton binding energies in these moderate-gap VODPs deserve closer scrutiny. To gain a deeper insight into the low-energy excitons, we examine their wave functions in both the reciprocal and real spaces. Within the Tamm-Dancoff approximation [45,68], the exciton wave functions can be expanded as a linear combination of products of the electron and hole wave functions $\psi_{c\boldsymbol{k}}(\boldsymbol{r_e})$ and $\psi_{v\boldsymbol{k}}(\boldsymbol{r_h})$:

$$\psi^S(\boldsymbol{r_e}, \boldsymbol{r_h}) = \sum_{k,c,v} A^s_{vc\boldsymbol{k}} \psi_{c\boldsymbol{k}}(\boldsymbol{r_e}) \psi^*_{v\boldsymbol{k}}(\boldsymbol{r_h}), \tag{1}$$

where S indexes the excitonic state and $A^S_{vc\boldsymbol{k}}$ are often called the *e-h* amplitudes, which give the weights of independent *e-h* pair states in an excitonic state S. We have analyzed the BZ distribution of the lowest-energy dark and bright excitons in VODPs by defining a k-dependent *e-h* amplitude $|\Psi_S(\boldsymbol{k})|^2 = \sum_{vc} |A^S_{vc\boldsymbol{k}}|^2$. The radii of the circles in Fig. 3(a) are proportional to $|\Psi_S(\boldsymbol{k})|^2$. In contrast to halide perovskites, in which the Wannier-Mott excitons are highly localized in small regions of the BZ [69–71], the low-energy excitons in Cs_2TiI_6 are far more extended in the BZ, as can be seen from Fig. 3(a). Therefore, the excitonic states can be accurately described even with a relatively coarse k grid. To further illustrate the Frenkel nature of the excitons, we compare $\Psi_S(\boldsymbol{k})$ with that of a hydrogenic model [72,73], $\Psi_{\rm hy}(\boldsymbol{k}) = (2a_0)^{\frac{3}{2}}/\pi(1 + a_0^2k^2)^2$, as shown in the inset of Fig. 3(a). The calculated $|\Psi_S(\boldsymbol{k})|^2$ of the lowest-energy exciton agrees reasonably with $|\Psi_{\rm hy}(\boldsymbol{k})|^2$ using very small Bohr radius $a_0 = 3.7$ a.u., suggesting a highly localized exciton in this system.

The localization of excitons can also be directly visualized in real space. To this end, we fix the hole position at an iodine atom, and plot the electron distribution of the lowest-energy dark and bright excitons for Cs_2TiI_6 in Fig. 3(b), which shows that the electron is mainly localized within one $[TiI_6]^{2-}$ octahedron. This conclusion does not change with different choices of the hole position, as shown in Fig. S7 of the Supplemental Material [50]. The fact that excitons are highly localized is in line with our previous analysis of the electronic structure, and the conclusion that Cs_2MX_6 can be considered as a 3D assembly of weakly coupled $[MX_6]^{2-}$ clusters, resulting in the formation of Frenkel excitons like those in molecular solids [74]. The electronic dielectric constants ε_∞ of Cs_2MX_6 range from 2.97 to 4.46 (Table I), which are very small compared to typical semiconductors such as Si or GaAs, but are comparable to other molecular solids such as naphthalene or anthracene [75] (Table S2 in Supplemental Material [50]). The relatively weak dielectric screening of Cs_2MX_6 also contributes to an overall strong *e-h* interaction, thus the exceptionally large exciton binding energies.

Finally, we would like to address possible exciton-phonon coupling effects on the calculated exciton binding energy. As recently shown by Filip *et al.* [76], exciton-phonon coupling can considerably renormalize the exciton binding energies in ionic materials. We estimate the correction (ΔE_b) to the exciton binding energy due to phonon-screening effects using a simplified formula [76]:

$$\Delta E_b = -2E_b \frac{\omega_{\rm LO}}{\omega_{\rm LO} + E_b}\left(1 - \frac{\varepsilon_\infty}{\varepsilon_0}\right), \tag{2}$$

where ϵ_∞ is the high-frequency dielectric constant, ϵ_0 is the static dielectric constant, and $\omega_{\rm LO}$ is the frequency of the dominant longitudinal optical (LO) phonon, which is usually the highest LO phonon. The phonon dispersions [77,78] of four VODPs are shown in Fig. S8 of the Supplemental Material [50]. We show in Table I the estimated ΔE_b, which are less than 50 meV for all four systems studied. Therefore, while

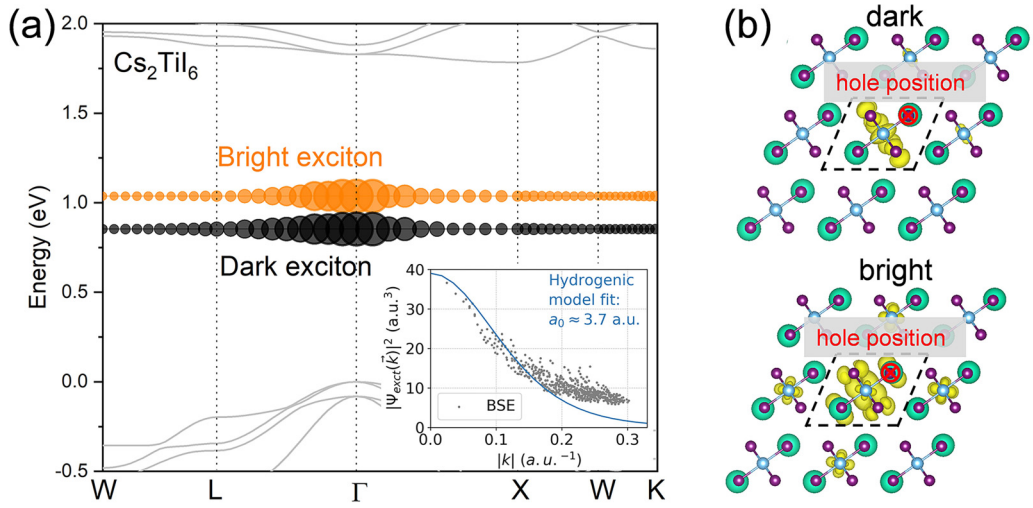

FIG. 3. (a) Reciprocal-space distribution of exciton wave functions of Cs_2TiI_6. The orange and black circles represent the lowest bright and dark excitons, respectively. The inset is a fitting of the exciton wave function with a hydrogenic model. (b) Real-space distribution of electrons for the lowest-energy dark and bright excitons. The hole position is fixed at an iodine atom. About 80% of the electron density is within the isosurface (shown in yellow).

these corrections are not negligible, they do not significantly affect our conclusion.

III. SUMMARY

In summary, we have predicted giant exciton binding energies ranging from 0.95 to 1.65 eV (after correction for the electron-phonon renormalization effects) in moderate-gap bulk VODP materials A_2MX_6 (A = Cs; M = Ti, Zr; X = I, Br). The exciton binding energies in these systems are one order of magnitude larger than typical inorganic semiconductors with comparable quasiparticle band gaps; they are even larger than those of monolayer transition metal dichalcogenides with similar fundamental band gaps. The lowest-energy excitons are dark, and the predicted absorption edges agree well with experiment, resolving an outstanding puzzle that the calculated (quasiparticle) band gaps seem to be much larger than the measured (optical) gaps. SOC effects play an important role in mixing the spin-singlet and spin-triplet excitons, resulting in a redshift to the absorption edges. We believe these materials provide a unique platform for exploring the properties and dynamics of Frenkel excitons, investigating more exotic composite quasiparticles such as biexcitons and trions, and realizing exciton-based optoelectronics devices. Our finding also paves the way for searching bulk semiconductors with extraordinarily strong *e-h* interaction. Two characteristics of such semiconductors are (1) the crystal structure should consist of weakly coupled building units (e.g., clusters, superatoms, or one-dimensional wires) and (2) the material should have relatively weak dielectric screening effects to ensure a strong Coulomb interaction between electrons and holes.

Note added. Recently, we became aware of computational studies by Kavanagh *et al.* [79] and Cucco *et al.* [80], which also show the large exciton binding energies in several vacancy-ordered double perovskites.

ACKNOWLEDGMENTS

This work is supported by the National Natural Science Foundation of China (Grants No. 12104080 and No. 91961204), the Fundamental Research Funds for the Central Universities (Grants No. DUT22LK04, and DUT22ZD103) and XingLiaoYingCai Project of Liaoning province, China (Grant No. XLYC1905014). Work at State University of New York at Buffalo (SUNYB) is supported by NSF Grant No. DMREF-1626967. The authors acknowledge the computer resources provided by the Supercomputing Center of Dalian University of Technology and the Center for Computational Research, SUNYB.

[1] X. Ai, E. W. Evans, S. Dong, A. J. Gillett, H. Guo, Y. Chen, T. J. H. Hele, R. H. Friend, and F. Li, Efficient radical-based light-emitting diodes with doublet emission, Nature (London) **563**, 536 (2018).

[2] K. Takanabe, Photocatalytic water splitting: quantitative approaches toward photocatalyst by design, ACS Catal. **7**, 8006 (2017).

[3] N. S. Ginsberg and W. A. Tisdale, Spatially resolved photogenerated exciton and charge transport in emerging semiconductors, Annu. Rev. Phys. Chem. **71**, 1 (2020).

[4] L. M. Herz, How lattice dynamics moderate the electronic properties of metal-halide perovskites, J. Phys. Chem. Lett. **9**, 6853 (2018).

[5] M. M. Ugeda, A. J. Bradley, S.-F. Shi, F. H. da Jornada, Y. Zhang, D. Y. Qiu, W. Ruan, S.-K. Mo, Z. Hussain, Z.-X. Shen, F. Wang, S. G. Louie, and M. F. Crommie, Giant bandgap renormalization and excitonic effects in a monolayer transition metal dichalcogenide semiconductor, Nat. Mater. **13**, 1091 (2014).

[6] H.-P. Komsa and A. V. Krasheninnikov, Effects of confinement and environment on the electronic structure and exciton

binding energy of MoS_2 from first principles, Phys. Rev. B **86**, 241201(R) (2012).

[7] A. Ramasubramaniam, Large excitonic effects in monolayers of molybdenum and tungsten dichalcogenides, Phys. Rev. B **86**, 115409 (2012).

[8] J. Feng, X. Qian, C.-W. Huang, and J. Li, Strain-engineered artificial atom as a broad-spectrum solar energy funnel, Nat. Photonics **6**, 866 (2012).

[9] J. Shang, X. Shen, C. Cong, N. Peimyoo, B. Cao, M. Eginligil, and T. Yu, Observation of excitonic fine structure in a 2D transition-metal dichalcogenide semiconductor, ACS Nano **9**, 647 (2015).

[10] Y. You, X.-X. Zhang, T. C. Berkelbach, M. S. Hybertsen, D. R. Reichman, and T. F. Heinz, Observation of biexcitons in monolayer WSe_2, Nat. Phys. **11**, 477 (2015).

[11] K. F. Mak, K. He, C. Lee, G. H. Lee, J. Hone, T. F. Heinz, and J. Shan, Tightly bound trions in monolayer MoS_2, Nat. Mater. **12**, 207 (2013).

[12] J. S. Ross, S. Wu, H. Yu, N. J. Ghimire, A. M. Jones, G. Aivazian, J. Yan, D. G. Mandrus, D. Xiao, W. Yao, and X. Xu, Electrical control of neutral and charged excitons in a monolayer semiconductor, Nat. Commun. **4**, 1474 (2013).

[13] S. Kéna-Cohen and S. R. Forrest, Room-temperature polariton lasing in an organic single-crystal microcavity, Nat. Photonics **4**, 371 (2010).

[14] J. D. Plumhof, T. Stöferle, L. Mai, U. Scherf, and R. F. Mahrt, Room-temperature Bose-Einstein condensation of cavity exciton-polaritons in a polymer, Nat. Mater. **13**, 247 (2014).

[15] J. Even, L. Pedesseau, and C. Katan, Understanding quantum confinement of charge carriers in layered 2D hybrid perovskites, Chem. Phys. Chem. **15**, 3733 (2014).

[16] B. Traore, L. Pedesseau, L. Assam, X. Che, J.-C. Blancon, H. Tsai, W. Nie, C. C. Stoumpos, M. G. Kanatzidis, S. Tretiak, A. D. Mohite, J. Even, M. Kepenekian, and C. Katan, Composite nature of layered hybrid perovskites: assessment on quantum and dielectric confinements and band alignment, ACS Nano **12**, 3321 (2018).

[17] D. B. Straus and C. R. Kagan, Electrons, excitons, and phonons in two-dimensional hybrid perovskites: Connecting structural, optical, and electronic properties, J. Phys. Chem. Lett. **9**, 1434 (2018).

[18] J.-H. Choi, P. Cui, H. Lan, and Z. Zhang, Linear Scaling of the Exciton Binding Energy Versus the Band Gap of Two-Dimensional Materials, Phys. Rev. Lett. **115**, 066403 (2015).

[19] L. Wirtz, A. Marini, and A. Rubio, Excitons in Boron Nitride Nanotubes: Dimensionality Effects, Phys. Rev. Lett. **96**, 126104 (2006).

[20] C. D. Spataru, S. Ismail-Beigi, L. X. Benedict, and S. G. Louie, Excitonic Effects and Optical Spectra of Single-Walled Carbon Nanotubes, Phys. Rev. Lett. **92**, 077402 (2004).

[21] D. Y. Qiu, F. H. da Jornada, and S. G. Louie, Optical Spectrum of MoS: Many-Body Effects and Diversity of Exciton States, Phys. Rev. Lett. **111**, 216805 (2013).

[22] E. L. Shirley, L. X. Benedict, and S. G. Louie, Excitons in solid C_{60}, Phys. Rev. B **54**, 10970 (1996).

[23] J. C. Grossman, M. Rohlfing, L. Mitas, S. G. Louie, and M. L. Cohen, High Accuracy Many-Body Calculational Approaches for Excitations in Molecules, Phys. Rev. Lett. **86**, 472 (2001).

[24] Y. Onodera and Y. Toyozawa, Excitons in alkali halides, J. Phys. Soc. Jpn. **22**, 833 (1967).

[25] R. T. Williams and K. S. Song, The self-trapped exciton, J. Phys. Chem. Solids **51**, 679 (1990).

[26] A. Trichet, F. Médard, J. Zúñiga-Pérez, B. Alloing, and M. Richard, From strong to weak coupling regime in a single GaN microwire up to room temperature, New J. Phys. **14**, 073004 (2012).

[27] S. Christopoulos, G. B. H. von Högersthal, A. J. D. Grundy, P. G. Lagoudakis, A. V. Kavokin, J. J. Baumberg, G. Christmann, R. Butté, E. Feltin, J.-F. Carlin, and N. Grandjean, Room-Temperature Polariton Lasing in Semiconductor Microcavities, Phys. Rev. Lett. **98**, 126405 (2007).

[28] T.-C. Lu, Y.-Y. Lai, Y.-P. Lan, S.-W. Huang, J.-R. Chen, Y.-C. Wu, W.-F. Hsieh, and H. Deng, Room temperature polariton lasing vs. photon lasing in a ZnO-based hybrid microcavity, Opt. Express **20**, 5530 (2012).

[29] D. Snoke and G. M. Kavoulakis, Bose-Einstein condensation of excitons in Cu_2O: Progress over 30 years, Rep. Prog. Phys. **77**, 116501 (2014).

[30] T. Kazimierczuk, D. Fröhlich, S. Scheel, H. Stolz, and M. Bayer, Giant Rydberg excitons in the copper oxide Cu_2O, Nature (London) **514**, 343 (2014).

[31] K. Saito, M. Hasuo, T. Hatano, and N. Nagasawa, Band gap energy and binding energies of Z3-excitions in CuCl, Solid State Commun. **94**, 33 (1995).

[32] R. Laskowski, N. E. Christensen, P. Blaha, and B. Palanivel, Strong excitonic effects in $CuAlO_2$ delafossite transparent conductive oxides, Phys. Rev. B **79**, 165209 (2009).

[33] H. Hiraga, T. Makino, T. Fukumura, A. Ohtomo, and M. Kawasaki, Excitonic characteristics in direct wide-band-gap $CuScO_2$ epitaxial thin films, Appl. Phys. Lett. **95**, 211908 (2009).

[34] B. Cai, X. Li, Y. Gu, M. Harb, J. Li, M. Xie, F. Cao, J. Song, S. Zhang, L. Cavallo, and H. Zeng, Quantum confinement effect of two-dimensional all-inorganic halide perovskites, Sci. China Mater. **60**, 811 (2017).

[35] Y.-F. Ding, Q.-Q. Zhao, Z.-L. Yu, Y.-Q. Zhao, B. Liu, P.-B. He, H. Zhou, K. Li, S.-F. Yin, and M.-Q. Cai, Strong thickness-dependent quantum confinement in all-inorganic perovskite Cs_2PbI_4 with a Ruddlesden-Popper structure, J. Mater. Chem. C **7**, 7433 (2019).

[36] Z. Yang, M. Wang, H. Qiu, X. Yao, X. Lao, S. Xu, Z. Lin, L. Sun, and J. Shao, Engineering the exciton dissociation in quantum-confined 2D $CsPbBr_3$ nanosheet films, Adv. Funct. Mater. **28**, 1705908 (2018).

[37] B. Cucco, G. Bouder, L. Pedesseau, C. Katan, J. Even, M. Kepenekian, and G. Volonakis, Electronic structure and stability of Cs_2TiX_6 and Cs_2ZrX_6 ($X = \mathrm{Br}, \mathrm{I}$) vacancy ordered double perovskites, Appl. Phys. Lett. **119**, 181903 (2021).

[38] A. E. Maughan, A. M. Ganose, D. O. Scanlon, and J. R. Neilson, Perspectives and design principles of vacancy-ordered double perovskite halide semiconductors, Chem. Mater. **31**, 1184 (2019).

[39] R. Sa, Q. Zhang, B. Luo, and D. Liu, Exploring the electronic and optical properties of vacancy-ordered double perovskites Cs_2PtX_6 ($X = \mathrm{Cl}, \mathrm{Br}, \mathrm{I}$), J. Solid State Chem. **304**, 122602 (2021).

[40] W. Kohn and L. J. Sham, Self-consistent equations including exchange and correlation effects, Phys. Rev. **140**, A1133 (1965).

[41] M. Giantomassi, M. Stankovski, R. Shaltaf, M. Grüning, F. Bruneval, P. Rinke, and G.-M. Rignanese, Electronic properties of interfaces and defects from many-body perturbation theory: Recent developments and applications, Phys. Status Solidi **248**, 275 (2011).

[42] G. Onida, L. Reining, and A. Rubio, Electronic excitations: Density-functional versus many-body Green's-function approaches, Rev. Mod. Phys. **74**, 601 (2002).

[43] M. S. Hybertsen and S. G. Louie, Electron correlation in semiconductors and insulators: Band gaps and quasiparticle energies, Phys. Rev. B **34**, 5390 (1986).

[44] M. Rohlfing and S. G. Louie, Electron-hole excitations and optical spectra from first principles, Phys. Rev. B **62**, 4927 (2000).

[45] J. Deslippe, G. Samsonidze, D. A. Strubbe, M. Jain, M. L. Cohen, and S. G. Louie, BerkeleyGW: A massively parallel computer package for the calculation of the quasiparticle and optical properties of materials and nanostructures, Comput. Phys. Commun. **183**, 1269 (2012).

[46] S. Lebègue, B. Arnaud, M. Alouani, and P. E. Bloechl, Implementation of an all-electron GW approximation based on the projector augmented wave method without plasmon pole approximation: Application to Si, SiC, AlAs, InAs, NaH, and KH, Phys. Rev. B **67**, 155208 (2003).

[47] J. Deslippe, G. Samsonidze, M. Jain, M. L. Cohen, and S. G. Louie, Coulomb-hole summations and energies for GW calculations with limited number of empty orbitals: A modified static remainder approach, Phys. Rev. B **87**, 165124 (2013).

[48] M. Rohlfing and S. G. Louie, Electron-Hole Excitations in Semiconductors and Insulators, Phys. Rev. Lett. **81**, 2312 (1998).

[49] M.-G. Ju, M. Chen, Y. Zhou, H. F. Garces, J. Dai, L. Ma, N. P. Padture, and X. C. Zeng, Earth-abundant nontoxic titanium(IV)-based vacancy-ordered double perovskite halides with tunable 1.0 to 1.8 eV bandgaps for photovoltaic applications, ACS Energy Lett. **3**, 297 (2018).

[50] See Supplemental Material at http://link.aps.org/supplemental/10.1103/PhysRevB.107.235119 for the computation methods; convergence behavior of the calculated excitonic properties; the optical absorption and excitonic structure of Cs2TiBr6, Cs2ZrI6, and Cs2ZrBr6; real-space distribution of electrons of Cs2TiI6 for the lowest-energy dark excitons with different hole positions; comparison of the electronic dielectric constants; phonon calculations; and the calculated absorption spectra of Cs2TiI6.

[51] J. P. Perdew, K. Burke, and M. Ernzerhof, Generalized Gradient Approximation Made Simple, Phys. Rev. Lett. **77**, 3865 (1996).

[52] P. Giannozzi, S. Baroni, N. Bonini, M. Calandra, R. Car, C. Cavazzoni, D. Ceresoli, G. L. Chiarotti, M. Cococcioni, I. Dabo, A. Dal Corso, S. De Gironcoli, S. Fabris, G. Fratesi, R. Gebauer, U. Gerstmann, C. Gougoussis, A. Kokalj, M. Lazzeri, L. Martin-Samos, N. Marzari, F. Mauri, R. Mazzarello, S. Paolini, A. Pasquarello, L. Paulatto, C. Sbraccia, S. Scandolo, G. Sclauzero, A. P. Seitsonen, A. Smogunov, P. Umari, and R. M. Wentzcovitch, QUANTUM ESPRESSO: A modular and open-source software project for quantum simulations of materials, J. Phys.: Condens. Matter **21**, 395502 (2009).

[53] D. R. Hamann, Optimized norm-conserving Vanderbilt pseudopotentials, Phys. Rev. B **88**, 085117 (2013).

[54] M. J. van Setten, M. Giantomassi, E. Bousquet, M. J. Verstraete, D. R. Hamann, X. Gonze, and G.-M. Rignanese, The PseudoDojo: Training and grading a 85 element optimized norm-conserving pseudopotential table, Comput. Phys. Commun. **226**, 39 (2018).

[55] W. Gao, X. Gao, T. A. Abtew, Y.-Y. Sun, S. Zhang, and P. Zhang, Quasiparticle band gap of organic-inorganic hybrid perovskites: Crystal structure, spin-orbit coupling, and self-energy effects, Phys. Rev. B **93**, 085202 (2016).

[56] P. Jena and Q. Sun, Super atomic clusters: Design rules and potential for building blocks of materials, Chem. Rev. **118**, 5755 (2018).

[57] M. Stankovski, G. Antonius, D. Waroquiers, A. Miglio, H. Dixit, K. Sankaran, M. Giantomassi, X. Gonze, M. Côté, and G.-M. Rignanese, G_0W_0 band gap of ZnO: Effects of plasmon-pole models, Phys. Rev. B **84**, 241201(R) (2011).

[58] C. Friedrich, M. C. Müller, and S. Blügel, Band convergence and linearization error correction of all-electron GW calculations: the extreme case of zinc oxide, Phys. Rev. B **83**, 081101(R) (2011).

[59] W. Gao, W. Xia, X. Gao, and P. Zhang, Speeding up GW calculations to meet the challenge of large scale quasiparticle predictions, Sci. Rep. **6**, 36849 (2016).

[60] B.-C. Shih, Y. Xue, P. Zhang, M. L. Cohen, and S. G. Louie, Quasiparticle Band Gap of ZnO: High Accuracy from the Conventional G_0W_0 Approach, Phys. Rev. Lett. **105**, 146401 (2010).

[61] M. S. Dresselhaus, G. Dresselhaus, and A. Jorio, *Applications of Group Theory to the Physics of Solids* (Springer, New York, 2008).

[62] D. Kammerlander, S. Botti, M. A. L. Marques, A. Marini, and C. Attaccalite, Speeding up the solution of the Bethe-Salpeter equation by a double-grid method and Wannier interpolation, Phys. Rev. B **86**, 125203 (2012).

[63] Z. Yang and C. A. Ullrich, Direct calculation of exciton binding energies with time-dependent density-functional theory, Phys. Rev. B **87**, 195204 (2013).

[64] K. A. Velizhanin and A. Saxena, Excitonic effects in two-dimensional semiconductors: Path integral Monte Carlo approach, Phys. Rev. B **92**, 195305 (2015).

[65] Z. Qiu, M. Trushin, H. Fang, I. Verzhbitskiy, S. Gao, E. Laksono, M. Yang, P. Lyu, J. Li, J. Su, M. Telychko, K. Watanabe, T. Taniguchi, J. Wu, A. H. C. Neto, L. Yang, G. Eda, S. Adam, and J. Lu, Giant gate-tunable bandgap renormalization and excitonic effects in a 2D semiconductor, Sci. Adv. **5**, eaaw2347 (2022).

[66] A. C. Riis-Jensen, T. Deilmann, T. Olsen, and K. S. Thygesen, Classifying the electronic and optical properties of janus monolayers, ACS Nano **13**, 13354 (2019).

[67] S. M. Liga and G. Konstantatos, Colloidal synthesis of lead-free $Cs_2TiBr_{6-x}I_x$ perovskite nanocrystals, J. Mater. Chem. C **9**, 11098 (2021).

[68] A. L. Fetter and J. D. Walecka, *Quantum Theory of Many-Particle Systems* (Courier, New York, 2012).

[69] J. Tilchin, D. N. Dirin, G. I. Maikov, A. Sashchiuk, M. V. Kovalenko, and E. Lifshitz, Hydrogen-like Wannier-Mott excitons in single crystal of methylammonium lead bromide perovskite, ACS Nano **10**, 6363 (2016).

[70] L. Huang and W. R. L. Lambrecht, Electronic band structure, phonons, and exciton binding energies of halide perovskites

$CsSnCl_3$, $CsSnBr_3$, and $CsSnI_3$, Phys. Rev. B **88**, 165203 (2013).

[71] J. M. Frost, K. T. Butler, F. Brivio, C. H. Hendon, M. van Schilfgaarde, and A. Walsh, Atomistic origins of high-performance in hybrid halide perovskite solar cells, Nano Lett. **14**, 2584 (2014).

[72] G. H. Wannier, The structure of electronic excitation levels in insulating crystals, Phys. Rev. **52**, 191 (1937).

[73] R. J. Elliott, Intensity of optical absorption by excitons, Phys. Rev. **108**, 1384 (1957).

[74] P. Cudazzo, F. Sottile, A. Rubio, and M. Gatti, Exciton dispersion in molecular solids, J. Phys. Condens. Matter **27**, 113204 (2015).

[75] M. Cardona and Y. Y. Peter, *Fundamentals of Semiconductors*, Vol. 619 (Springer, New York, 2005); M. Pope and C. E. Swenberg, *Electronic Processes in Organic Crystals and Polymers*, Vol. 56 (Oxford University Press, Oxford, 1999). T. Suthan, N. P. Rajesh, P. V. Dhanaraj, and C. K. Mahadevan, Growth and characterization of naphthalene single crystals grown by modified vertical Bridgman method, Spectrochim. Acta, Part A **75**, 69 (2010).

[76] M. R. Filip, J. B. Haber, and J. B. Neaton, Phonon Screening of Excitons in Semiconductors: Halide Perovskites and Beyond, Phys. Rev. Lett. **127**, 067401 (2021).

[77] S. Baroni, S. de Gironcoli, A. Dal Corso, and P. Giannozzi, Phonons and related crystal properties from density-functional perturbation theory, Rev. Mod. Phys. **73**, 515 (2001).

[78] A. Togo and I. Tanaka, First principles phonon calculations in materials science, Scr. Mater. **108**, 1 (2015).

[79] S. R. Kavanagh, C. N. Savory, S. M. Liga, G. Konstantatos, A. Walsh, and D. O. Scanlon, Frenkel excitons in vacancy-ordered titanium halide perovskites (Cs_2TiX_6), J. Phys. Chem. Lett. **13**, 10965 (2022).

[80] B. Cucco, C. Katan, J. Even, M. Kepenekian, and G. Volonakis, Fine structure of excitons in vacancy-ordered halide double perovskites, ACS Mater. Lett. **5**, 52 (2023).